PAPER

Check for updates

Luminescent zinc(II) selone macrocyclic ring†

Ganesan Prabusankar, [ID] *[a] Gembali Raju,[a] Moulali Vaddamanu,[a]
Nirmala Muthukumaran,[a] Arruri Sathyanarayana,[b] Shin-ya Nakamura,[b]
Yamane Masaya,[b] Kyohei Hisano,[b] Osamu Tsutsumi, [ID] [b] Chinmoy Biswas[c]
and Sai Santosh Kumar Raavi [ID] [c]

The synthesis and photophysical properties of macrocyclic Zn(II) selone molecule have been reported. The structural property of Zn(II) selone was elucidated using single crystal X-ray diffraction study. The solid-state structure of zinc(II) selone molecule exhibits a perfect zinc(II) selone 28 membered ring system with tetra coordination geometry around zinc(II) center. The zinc(II) selone ring system can be considered as the largest zinc(II) ring system known without any non-interacting centered guest moiety. Detailed trends in photophysical as well as thermal properties were probed. In photoluminescence study, the solid-state sample of zinc(II) selone ring system emits the bluish-yellow color with considerable quantum yields, while the solution state sample of zinc(II) selone ring system in DMSO emits bluish-yellow. The luminescence lifetime of zinc(II) selone was measured using standard time-correlated single photon counting (TCSPC) technique.

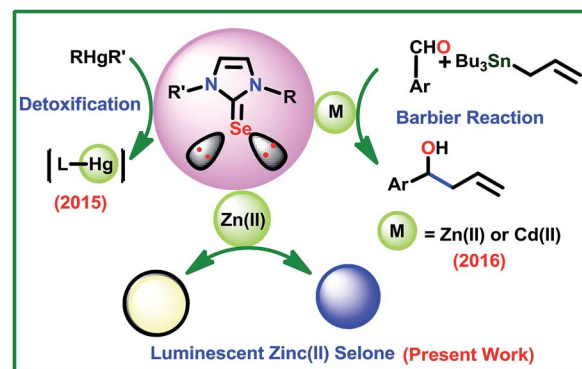## 1 Introduction

The chemistry of imidazoline-2-selone (IMSe) metal coordination compounds has attracted much attention owing to their unusual structural features and their applications in catalysis,[1–3] nano science,[3–5] and medicinal chemistry.[5,6] Several metal-IMSe derivatives have been isolated and demonstrated for these applications. IMSe can be considered as a potential neutral donor ligand in metal coordination compound formation due to the versatile electronic and steric properties of ligands. However, the application of IMSe coordinated group d[10] metal derivatives is not explored much (Scheme 1). For example, the hexagonal and cubic ZnSe were derived from the $[(DIS)ZnCl_2]$ (DIS = 1,3-dimethyl-2(3H)-imidazoleselone) as synthon under a larger scale thermolytic decomposition route in 2002.[4] Parkin et al. reported the detoxification of mercury compounds using 1-methyl-1,3-dihydro-2H-benzimidazole-2-selone by photolytically cleaving mercury–carbon bonds.[7] Similarly, the highly toxic organomercury compounds such as ArHgOH and RHgC were converted as less toxic HgE nanoparticles using N-methyl-N'-

ethanol imidazoline-2-thione and N-methyl-N'-ethanol imidazoline-2-selone.[8] Recently we have demonstrated the catalytic application of cadmium and zinc selones, $[(L^a)Cd(Cl)(NO_3)]$, $[\{(L^a)_4Cd\}^{2+}\{ClO_4\}_2{}^{2-}\cdot H_2O]$, $[\{(L^a)_4Zn\}^{2+}\{ClO_4\}_2{}^{2-}]$, $[(L^b)CdCl_2]_n$, $[\{(L^b)Cd(Cl)\}\{ClO_4\}]$ and $[\{(L^b)_2Zn\}\{ClO_4\}_2\cdot 2H_2O]$, ($L^a$ = 1-(2,6-diisopropyl phenol)-3-(2-methoxy-2-oxethyl)-imidazoline selone; L^b = 3-(2-methoxy-2-oxethyl)-1-mesityl-imidazoline selone) in Barbier type reactions.[9] Therefore, the N substituent in IMSe plays a crucial role in the application of the final coordination compound or materials.

Though the coordination chemistry of Zn(II)-IMSe is well established by Singh et al.,[10,11] the potential of these Zn(II)-IMSe derivatives are yet to explore.[4,9] Continuing our interest in the related area,[9] herein we report a simple strategy to isolate the luminescent Zn(II)-IMSe derived from chromophore tagged

[a]Department of Chemistry, Indian Institute of Technology Hyderabad, India-502 285. E-mail: prabu@iith.ac.in

[b]Department of Applied Chemistry, Ritsumeikan University, 1-1-1 Nojihigashi, Kusatsu 525-8577, Japan

[c]Department of Physics, Indian Institute of Technology Hyderabad, India-502 285

Scheme 1 Known applications of IMSe coordination compounds of d[10] metal derivatives.

IMSe. The macrocyclic zinc(II) selone ring molecule $[(\mu^2\text{-}\mathbf{1})ZnBr_2]_2$ (**2**) was conveniently derived from the reaction between [4,5-bis{(N-isopropylimidazol-2-selone)methyl}-acridine] (**1**) and $ZnBr_2$. The molecule **2** was fully characterized by CHN analysis, FT-IR, multinuclear (^{1}H and ^{13}C) NMR, TGA, UV-vis, fluorescence and single crystal X-ray diffraction techniques.

2   Results and discussion

Synthesis and characterization of 1

The molecule **1** was isolated in excellent yield from the reaction between [4,5-bis{(N-isopropyl imidazolium)methyl}-acridine] dibromide (**L**) and selenium powder in the presence of potassium carbonate (Scheme 2). The molecule **1** was characterized by FT-IR, multinuclear (^{1}H and ^{13}C) NMR, and single crystal X-ray diffraction technique. The seleniation of **L** was confirmed by NMR. Upon seleniation, the imidazolium C–H proton disappeared in the ^{1}H NMR, while the ^{13}C NMR chemical shift value of N–CH–N got downfield shifted from 135.48 ppm (for **L**)[12,13] to 154.78 ppm (N–C(Se)–N of **1**). Notably, the semi seleniated product was not observed in this reaction. The solid-state structure of **1** was determined by the single crystal X-ray diffraction technique.

The solid-state structure of **1** along with selected bond lengths and bond angles are reported in Fig. 1 and Table 1. Compound **1** represents the first imidazole chalcogenone derivative isolated with acridine back-bone. The imidazole selone moieties are *trans* to each other with respect to the acridine ring plane. The C=Se bond distances are almost the same (C(1)–Se(1), 1.832(5) Å and C(24)–Se(2), 1.833(4) Å). The Se=C bond distances are comparable with that of IMes = Se (IMes = C{(CH)(2,4,6-Me$_3$C$_6$H$_2$N)}$_2$) (1.827(6) Å).[14] The comparable N–C bond distances (N(1)–C(1), 1.356(6) Å; N(1)–C(2), 1.355(5) Å; N(3)–C(24), 1.355(5) Å and N(4)–C(24), 1.351(4) Å) in **1** implies that the existence of considerable π-overlap between nitrogen and carbon of N–C(Se)–N. The N–C(Se)–N bond angles
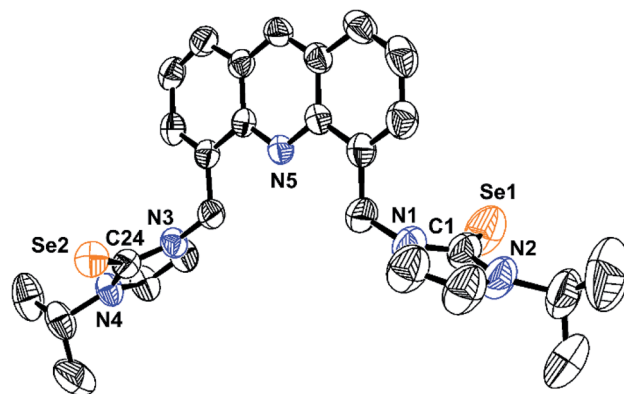

Fig. 1   The molecular structure of **1**. The hydrogen atoms have been omitted for the clarity. The selected bond lengths (Å) and bond angles (°): C(1)–Se(1), 1.832(5); C(24)–Se(2), 1.833(4); N(1)–C(1), 1.356(6); N(1)–C(2), 1.355(5); N(3)–C(24), 1.355(5); N(4)–C(24), 1.351(4); N(1)–C(1)–N(2), 104.9(4) and N(3)–C(24)–N(4), 105.5(3).

are nearly comparable (N(1)–C(1)–N(2), 104.9(4)° and N(3)–C(24)–N(4),105.5(3)°).
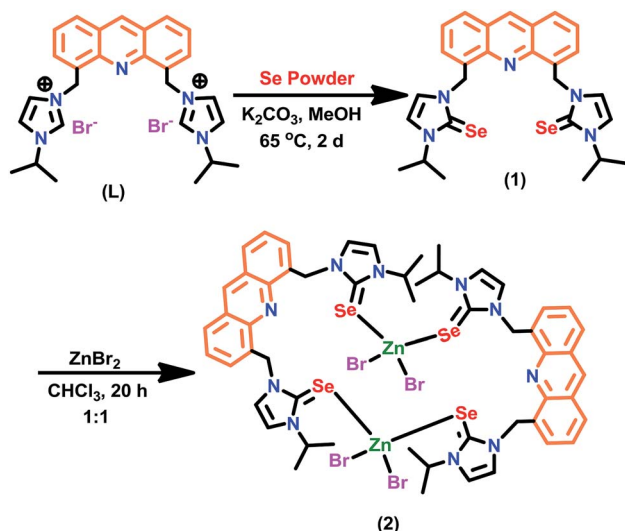
Synthesis and characterization of 2

The [(**1**)ZnBr$_2$]$_2$ (**2**) was isolated in very good yield (67%) from the direct reaction between **1** and zinc(II) bromide. **2** was characterized by CHN analysis, FT-IR, multinuclear (^{1}H and ^{13}C) NMR, TGA, UV-vis, fluorescence and single crystal X-ray diffraction techniques. Upon coordination, a slight upfield shift was observed in the ^{13}C NMR for N–C(Se)–N in **2** (154.42 ppm) compared to **1** (154.78 ppm).

Besides, the thermal stability of **2** was investigated from 30 °C to 800 °C (Fig. 2). **2** undergoes gradual decomposition through three steps. The initial weight loss till 94 °C with 6% can be attributed to the loss of partial decomposition of isopropyl group in **2**. Later **2** shows 26% weight loss till 430 °C due to the loss of halides along with a part of organic moieties. Moreover, the major weight loss was observed from 430 °C to 720 °C for the decomposition of organic moieties with a fraction of selenium moiety to yield ZnSe residue (found 9%, calcd 9%, see ESI†).

X-ray crystal structure of 2

The solid state structure of **2** was confirmed by single crystal X-ray diffraction technique. The dinuclear zinc-selone **2** crystallized in the monoclinic space group, $P2_n/n$. The solid-state structure with selected bond lengths and bond angles are reported in Fig. 3. The crystallographic data for **2** is furnished in Table 1. The molecule **2** is a dinuclear macrocyclic ring system with μ^2 bridged acridine imidazole selone linker. Though eleven zinc(II)-imidazole chalcogenone derivatives are known,[4,9–11] the chromophore tagged zinc(II)-imidazole chalcogenones are not isolated. **2** represent the first zinc(II)-imidazole selone tagged with acridine chromophore.

The zinc center in **2** is tetra coordinated by two bromide ions and two selones. The geometry of zinc(II) can be described as

Scheme 2   Synthesis of **1** and **2**.

Table 1 Crystal data and structure refinement parameters for 1 and 2

	1	2[a]
Empirical formula	$C_{3.38}H_{3.63}N_{0.63}Se_{0.25}$	$C_{27}H_{29}N_5ZnSe_2Br_2$
Formula weight	581.48	1613.37
T (K)	293	293
Crystal system	Orthorhombic	Monoclinic
Space group	$Pbca$	$P2_1/n$
Unit cell dimensions		
a (Å)	16.0791(3)	11.5441(9)
b (Å)	11.5168(2)	14.9994(13)
c (Å)	29.4333(6)	18.5505(18)
α (°)	—	—
β (°)	—	105.613(9)
γ (°)	—	—
Volume (Å³)	5450.48(19)	3093.6(5)
Z	8	12
Density (calculated) Mg m⁻³	1.4171	1.7319
Absorption coefficient mm⁻¹	3.568	7.008
$F(000)$	2344.3	1560.6
Scan range for data collection (deg)	6 to 141.74	7.7 to 145.46
Index ranges	$-16 \leq h \leq 19$	$-14 \leq h \leq 13$
	$-13 \leq k \leq 13$	$-18 \leq k \leq 17$
	$-35 \leq l \leq 26$	$-22 \leq l \leq 18$
Reflections collected/unique, R_{int}	14 786/5164/0.0321	12 465/5798/0.0396
Data/restraints/parameters	5164/0/311	5798/0/338
Goodness-of-fit on F^2	1.042	1.038
Final R indices $[I > 2\sigma(I)]^a$	$R_1 = 0.0515$	$R_1 = 0.0524$
	$wR_2 = 0.1503$	$wR_2 = 0.1272$
R indices (all data)	$R_1 = 0.0712$	$R_1 = 0.0815$
	$wR_2 = 0.1786$	$wR_2 = 0.1676$

[a] Symmetry code: $2 - X, -Y, -Z$.

a distorted tetrahedron. The Se–Zn–Se bond angle is 106.56(4)° and Br–Zn–Br bond angle is 112.40(6)°. The Se–Zn–Se bond angle in 2 is nearly comparable with that of $[\{(MOMS)_2Zn\}\{ClO_4\}_2·2H_2O]$ (MOMS = 3-(2-methoxy-2-oxoethyl)-1-mesityl-imidazoline selone) (103.05(5)°)[9] and $[(DIS)ZnCl_2]$ (DIS = 1,3-dimethyl-2(3H)-imidazoleselone) (103.58 (2)°).[4] The Br–Zn–Se bond angles are not comparable. The Se2–Zn1–Br2 (111.95(6)°) bond angle is considerably wider than that of Se1–Zn1–Br1

(109.92(5)°), Se2–Zn1–Br1 (108.30(4)°) and Se1–Zn1–Br2 (107.55(5)°) bond angles. The Zn–Br bond distances are not comparable. The Zn1–Br1 bond distance (2.409(13) Å) is slightly longer than that of Zn1–Br2 bond distance (2.368(14) Å). The Zn1–Se1 bond length (2.478(12) Å) is considerably longer than the Zn1–Se2 (2.492(12) Å) bond distance.

The Zn–Se bond distances in 2 is comparable with that of Zn–Se (neutral donor site) four-membered ring $[(DDP)ZnSePh]_2$ (DDP = $HC[C(Me)N(2,4,6-Me_3C_6H_2)]_2$) (2.429(5) and 2.595(6) Å).[15a] However, the Zn–Se bond distances found in 2 is considerably longer than that of $[\{(MOMS)_2Zn\}\{ClO_4\}_2·2H_2O]$ (2.328(10) Å).[9] The C7 = Se1 bond distance (1.896(7) Å) is slightly longer than the C1 = Se2 bond distance (1.869(7) Å). Upon coordination with zinc(II), the C=Se bond distances in 2 are considerably elongated compared to 1. The distance between the two Zn(II) centers in 2 is 8.582 Å. The distance between two nitrogen atoms of acridine moieties in 2 is 9.082 Å. Notably, 2 represent a rare structurally characterized zinc-selone ring system composed of twenty eight atoms. As shown in Fig. 3(II), the acridine moiety helps the molecule 2 to maintain the perfect geometrical orientation. The molecule 2 is the largest zinc(II) ring system known without any non-interacting centered guest moiety. Interestingly the molecular packing of 2 depicts a channel like arrangement of molecules without any inter or intra molecular interactions (Fig. 4). As depicted along X axis, the molecules are closely packed in the ruptured
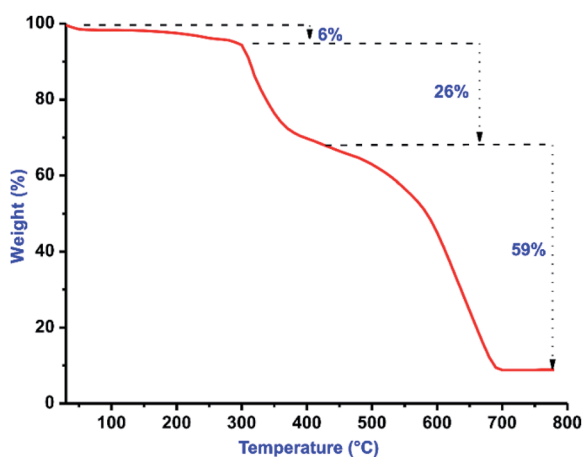

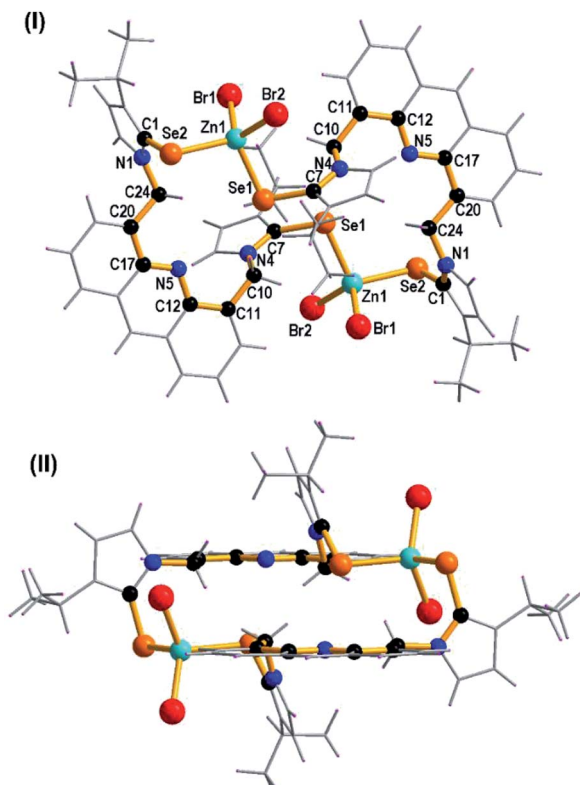Fig. 2 TGA curve of 2 from 30 to 800 °C under a nitrogen atmosphere with a heating rate of 10 °C min⁻¹.

Fig. 3 (I) The molecular structure of **2**. (II) The side view of molecular ring in **2**. The selected bond lengths (Å) and bond angles (°): Zn(1)–Se(1), 2.478(12); Zn(1)–Se(2), 2.492(12); Zn(1)–Br(1), 2.410(13); Zn(1)–Br(2), 2.368(14); C(1)–Se(2), 1.869(7); Se(1)–C(7), 1.896(7); N(1)–C(1), 1.352(9); N(2)–C(1), 1.339(8); N(3)–C(7), 1.328(9); N(4)–C(7), 1.337(8); Se(1)–Zn(1)–Se(2), 106.56(4); C(1)–Se(2)–Zn(1), 96.3(2); C(7)–Se(1)–Zn(1), 97.0(2); N(2)–C(1)–N(1), 106.7(6) and N(3)–C(7)–N(4), 107.3(6).

herringbone pattern. **2** depicts a strong face-to-face (N-facing opposite) acridine–acridine π···π interaction (3.356 Å and 3.378 Å) (see ESI†).[15b] Besides, a strong Br···H–C hydrogen bonding interaction is observed (2.959 Å and 2.927 Å). One of the isopropyl C–H group shows a weak hydrogen bonding interaction with acridine C–H (see ESI†).

Photophysical properties of 1 and 2

The solution state photophysical properties of **1** and **2** were investigated in DMSO using UV-vis and fluorescence spectroscopy. The UV-vis absorption spectra of **1** and **2** normalized at their longer wavelength absorption bands were shown in the Fig. 5. Both **1** and **2** exhibits a similar sharp band absorption spectra from 250 nm to 315 nm and broad band absorption spectra from 315 nm to 420 nm. The similar absorption pattern of **1** and **2** may be attributed to the partial dissociation of **2** in solution to result the mixture of coordination compounds with some ligands replaced by solvent, including mononuclear coordination compound, and original coordination compound. Based on the literature report[16–18] and the time-dependent density functional theory (TDDFT) of similar such system, 4,5-bis[(N-aryl-imidazole-2-ylidene)methyl]acridine silver(I) hexafluorophosphate,[18b] the absorption band from 250 nm to
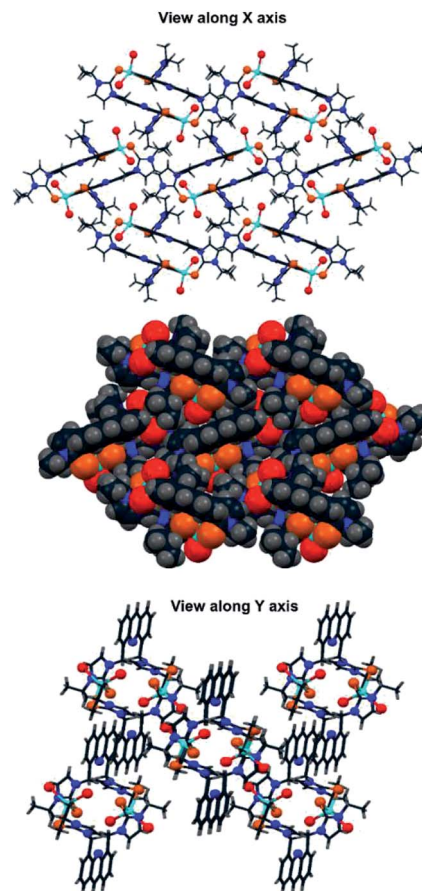

Fig. 4 The molecular packing of **2**. View along X axis and Y axis.

315 nm and 315 nm to 420 nm can be attributed to π → π* transition of acridine moiety. To understand the DMSO interference in UV-vis absorption study, the UV-vis absorption study was carried out for **2** in MeCN, MeOH, and CHCl₃ (see ESI Fig. S10†). However, there is no appreciable change in the absorption spectrum of **2** in DMSO vs. mixture of solvents.

The molar extinction coefficient of **1** and **2** was calculated at 259 nm and 358 nm using Beer–Lambert law (Fig. 6(i)–(iv)).
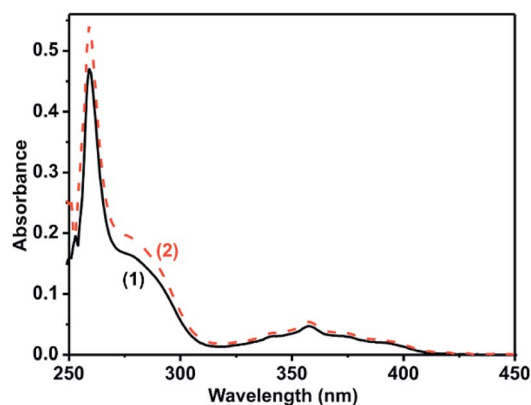

Fig. 5 Absorption spectra of **1** (solid line, black) and **2** (Broken line, red). 4×10^{-6} M in DMSO.
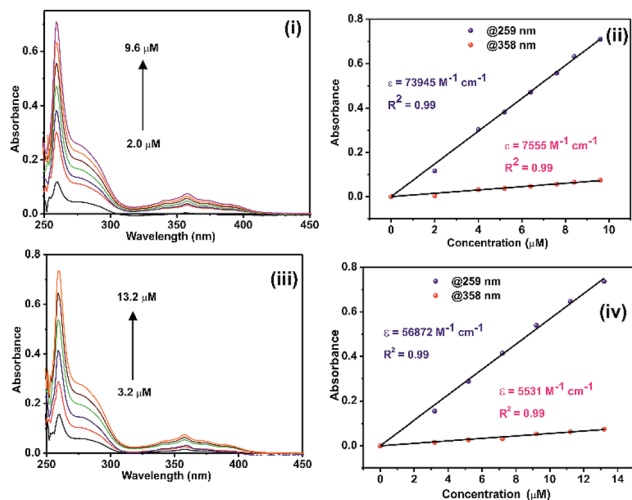
Fig. 6 (i) Absorption spectra of **1** at various concentrations, (ii) linear plot for the calculation of molar extinction coefficient of **1**, (iii) absorption spectra of **2** at various concentrations, (iv) linear plot for the calculation of molar extinction coefficient of **2**. Solvent: DMSO.

Plotting the absorbance of the analyte against its concentration yields a straight line with an excellent correlation coefficient (Fig. 6). The molar extinction coefficient of **1** and **2** were graphically calculated from the slopes of Fig. 6(ii) and (iv) and are found to be $7.4 \times 10^4 \ M^{-1} \ cm^{-1}$ and $7.6 \times 10^3 \ M^{-1} \ cm^{-1}$ for **1** and $5.7 \times 10^4 \ M^{-1} \ cm^{-1}$ and $5.5 \times 10^3 \ M^{-1} \ cm^{-1}$ for **2**. It is noteworthy that the extinction coefficient of **2** is lower than that of **1**. This may be due to the heavier atom effects.

The photoluminescence property of **1** and **2** was investigated in DMSO (Fig. 7 and see ESI†). The coordination compound **2** displayed photoluminescence at 347 and 363 nm in DMSO solution. These emissions are due to the ligand-based π–π* or metal-to-ligand charge transfer (MLCT) transitions.[19,20] Moreover the solution state emission properties of **1** are nearly comparable to **2** (see ESI†). This may be due to the partial dissociation of **2** in solution to result in the mixture of coordination compounds with some ligands replaced by solvent, including mononuclear coordination compound, and original coordination compound.

In solution state, the emission of **1** shows as increasing concentration increases the emission intensity and broadness of spectra (see ESI†). This can be attributed to aggregation induced emission (AIE).[21–23] However, on the other hand, **2** depicts an increase in emission intensity by increasing concentration up to 30×10^{-6} M, then emission intensity decreases and finally quenches (see ESI†). This observation could be attributed to the aggregation-caused quenching (ACQ) due to presence strong face-to-face (N-facing opposite) acridine–acridine π···π interaction (*vide supra*).[20–23] Similar face-to-face (N-facing opposite) acridine–acridine π···π interaction is also present in **1**. However, the AIE property of **1** in the solution can be attributed to the less favorable π···π stacking due to free molecular motion, while similar such mechanism is not possible in **2**.

The solid-state photoluminescence properties of **1** and **2** are considerably different from that of solution state nature (Fig. 8
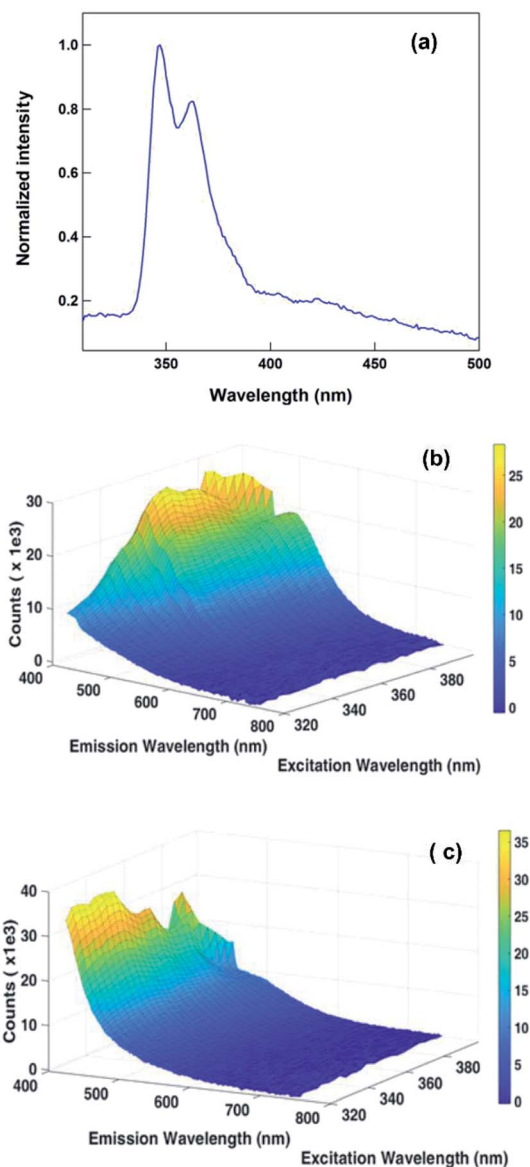

Fig. 7 (a) The solution state emission spectrum of **2** in DMSO (4×10^{-6} M). Excited at 260 nm; (b) 3D fluorescence spectrum of **1** in DMSO; (c) 3D fluorescence spectrum of **2** in DMSO.

and see ESI†). Notably, a significant difference was observed in the luminescence behavior of **2** in dilute solution and solid phase (Fig. 8a). This can be attributed to the different molecular association in the solution state compared to the solid state (*vide supra*). A broad emission band from 430 to 784 nm may be attributed to the solid packing mode of **2**. Consequently, bluish-yellow photoluminescence could be seen with the naked eye upon UV irradiation of the solid **2** at 365 nm (Fig. 8a, inset). The excitation at 397 nm shows the maximum intensity of emission at 487 nm (see ESI†). On the other hand when this compound was excited at 320 nm and 330 nm, the emission shape did not change, but the emission intensity tends to be lower than at excited wavelength 397 nm. From this study, we can conclude that the complex emission is excitation independent.

Also, to understand the nature of fluorescence emission maxima, we have investigated the 3D fluorescence study for **1**
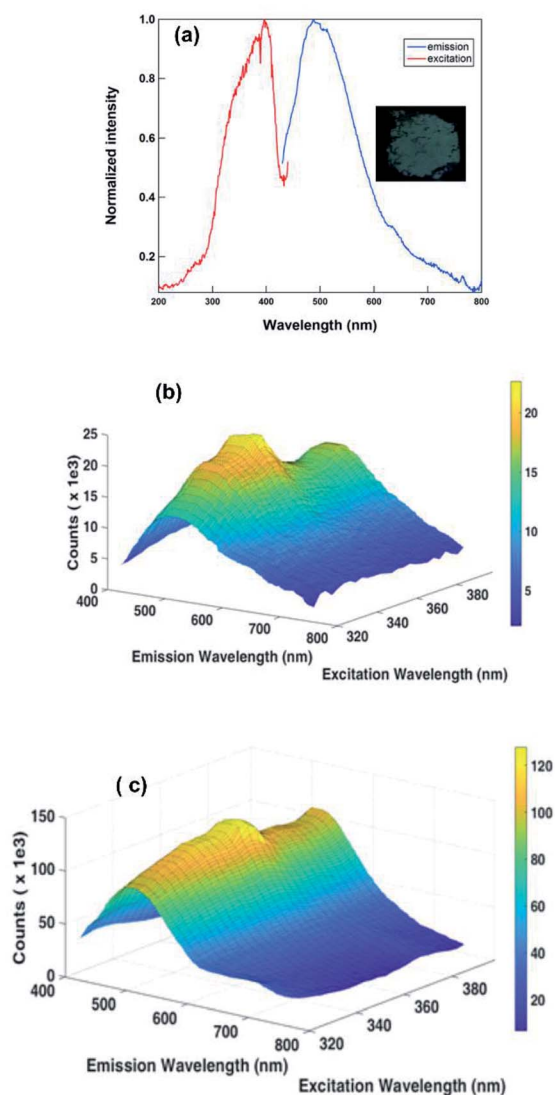
Fig. 9 The CIE chromaticity diagram for solution state and solid-state photoluminescence.

Fig. 8 (a) Emission (blue line, λ_{ex} = 397 nm) spectra of **2** in the solid state at room temperature (red line is excitation spectra, λ_{em} = 486 nm) and inset: photographic image of solid-state sample under UV irradiation at 365 nm; (b) 3D fluorescence spectrum of **1** in film mode; (c) 3D fluorescence spectrum of **2** in film mode.

mechanism of photoluminescence nature of **2** is aggregation specific as observed in similar such examples.[21–25]

Notably, the coordination compound **2** exhibited luminescence with relatively low quantum yields (Φ), even at room temperature in the air: total Φ was 0.67% for **2**, in the solid state. This could be due to the quenching effects of heavier selenium fragments present in **2**. Similar such co-existing molecular effect is not unusual in zinc(II) luminescent molecules.[26]

The luminescence lifetime of **2** was measured using standard time-correlated single photon counting (TCSPC) technique. The decay kinetic along with the instrument response function (IRF) at the steady-state emission peak λ_{em} = 528 nm is shown in Fig. 10. The decay is fitted using reconvolution fit analysis using the IRF to extract the life-time parameters from the whole time resolved measurement. The estimated lifetime values are 0.35 ns, 1.36 ns and 4.45 ns with the fit quality parameter χ^2 = 1.184 indicating best fit. The observed

and **2** in solution state as well as in solid state at different excitation wavelengths. The intensity was plotted as a function of excitation wavelength and emission wavelength. As shown in Fig. 7c, 8b and c, the emission property is independent of exitation nature, while **1** in solution is dependent. At this stage, we are unclear about the reason for excitation-dependent emission nature of **1** in solution.

The Commission Internationale de l'Eclairage (CIE) chromaticity diagram allows for quantitative evaluation of photoluminescence color as shown in Fig. 9. The photoluminescence color of solution state and solid-state are not comparable. A considerable change in the luminescence spectrum and color were observed between solution state and solid state. The solid-state sample of **2** emits the bluish-yellow color, while the solution state sample of **2** in DMSO emits blue. Thus, the
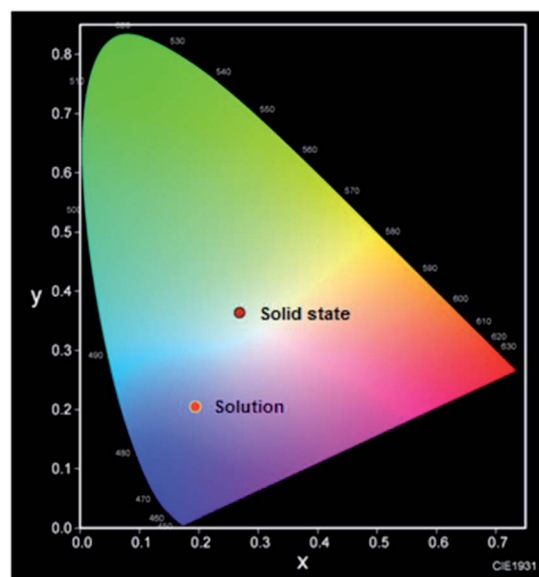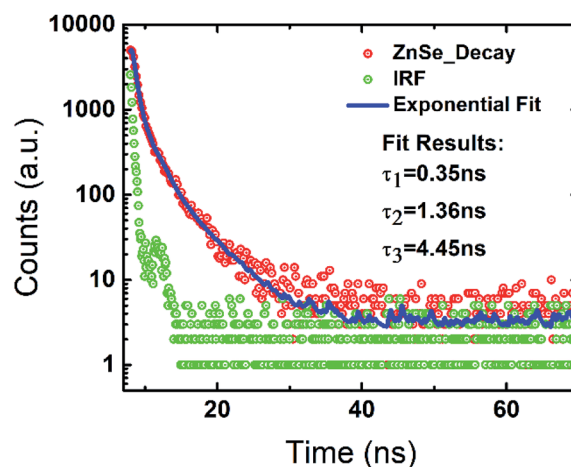

Fig. 10 Decay kinetic with IRF and reconvolution fit at 528 nm emission peak.

luminescence efficiency of **2** indicates the dominant nature of nonradiative recombination.[27] Considering the short lifetime, this molecule may find application in various optoelectronic applications like switching. In addition, the estimated quantum yields also suggest application as fluorescent marker. More investigations are underway to explore the various application of this class of luminescent molecules.

3 Experimental

Synthesis of 1

A mixture of **L** (400 mg, 0.68 mmol) and Se powder (162 mg, 2.05 mmol) and K_2CO_3 (378 mg, 2.73 mmol) in methanol (8 mL) was refluxed for 2 days under argon atmosphere. The volatiles were evaporated under vacuum, the resulting residue was dissolved in DCM (5 × 20 mL) and washed with water (50 mL). Subsequently, the organic layer was separated, dried with Na_2SO_4 then the volatiles were evaporated to get yellow solid of **1**. The further crystallization from $CHCl_3$ gave a pure form of **1**. Yield: 87% (based on **L**). Mp: 225–230 °C. CHN analysis for $C_{27}H_{29}N_5Se_2$ (MW: 581.47): calcd C, 55.77; H, 5.03; N, 12.04; found C, 56.0; H, 4.9; N, 11.9. FT-IR (cm^{-1}, neat): 3391(b), 3167(w), 3123(w), 3061(w), 2968(w), 2918(m), 2850(m), 1620(w), 1566(w), 1460(w), 1405(s), 1368(w), 1321(m), 1293(w), 1267(w), 1223(m), 1200(w), 1177(w), 1139(w), 1114(m), 821(m), 763(m), 731(s), 667(s), 618(m), 537(w). ^{1}H NMR (400 MHz, CDCl$_3$) δ: 8.76 (s, 1H, Ar–H), 7.94–7.92 (d, 2H, Im–H), 7.78–7.76 (d, 2H, Im–H), 7.48–7.45 (t, 2H, Ar–H), 7.14–7.13 (d, 2H, Ar–H), 6.88–6.87 (d, 2H, Ar–H), 6.20 (s, 4H, –CH_2), 5.30–5.20 (septet, 2H, –CH), 1.39–1.38 (d, 12H, –CH_3). ^{13}C NMR (100 MHz, CDCl$_3$) δ: 154.78 (*C*–Se), 146.16 (Ar–*C*), 136.84, 133.73, 130.36, 128.36, 126.39, 125.70, 119.99, 115.03, 53.37, 51.08, 48.63 (–*C*H$_2$), 21.97 (–*C*H$_3$).

Synthesis of 2

To a mixture of **1** (70 mg, 0.12 mmol), $ZnBr_2$ (28 mg, 0.12 mmol), $CHCl_3$ (10 mL) was added and refluxed for 20 h under argon atmosphere. The resultant yellow mixture was filtered and the precipitate was dissolved in mixture of acetonitrile, methanol and chloroform (2 : 1 : 0.5) to isolate yellow crystals of **2** at room temperature. Yield: 67% (based on **1**). CHN analysis for $C_{54}H_{58}N_{10}Br_4Se_4Zn_2$ (MW: 1613.32): calcd C, 40.20; H, 3.62; N, 8.68; found C, 40.1; H, 3.5; N, 8.6. Mp: 205–210 °C. FT-IR (cm^{-1}, neat): 3408(b), 3142(w), 3107(w), 2964(w), 2921(s), 2852(m), 1617(s), 1560(w), 1537(m), 1459(m), 1406(m), 1304(w), 1234(m), 1195(s), 1132(m), 1074(w), 1049(w), 971(w), 915(m), 884(w), 757(s), 722(m), 673(m), 614(w). ^{1}H NMR (400 MHz, DMSO-d_6) δ: 9.24 (s, 1H, Ar–H), 8.20–8.18 (d, 2H, Ar–H), 7.65–7.62 (t, 2H, Ar–H), 7.54–7.53 (d, 2H, Ar–H), 7.47–7.45 (t, 4H, Im–H), 6.16 (s, 4H, –CH_2), 5.14–5.04 (septet, 2H, –CH), 1.40–1.38 (d, 12H, –CH_3). ^{13}C NMR (100 MHz, DMSO-d_6) δ: 154.42 (*C*–Se), 145.60 (Ar–*C*), 137.48, 134.16, 129.23, 128.42, 126.22, 125.90, 120.63, 116.59, 50.79, 48.63 (–*C*H$_2$), 21.59 (–*C*H$_3$).

4 Conclusions

In conclusion, the acridine tagged bis imidazole-2-selone was isolated and fully characterized. The macrocyclic zinc(II) selone ring system (**2**) containing acridine tagged imidazole selone ligand was derived from the reaction between **1** and $ZnBr_2$ salt. The molecule **2** was characterized by elemental analysis, FTIR, NMR, UV-vis, fluorescence, time-correlated single photon counting, TGA, and single crystal X-ray diffraction techniques. **2** represents the structurally characterized zinc-selone ring system composed of twenty-eight atoms with unique molecular packing. Besides, **2** is the largest zinc(II) ring system known without any non-interacting centered guest moiety. The solid-state sample of **2** emits the bluish-yellow color with estimated quantum yields (Φ) of 0.67% and considerable lifetime values. We are currently exploring the emission properties of **2** concerning the guest association.

Conflicts of interest

There are no conflicts to declare.

Notes and references

1 (a) L. M. Zhang, H. Y. Li, H. X. Li, D. J. Young, Y. Wang and J. P. Lang, *Inorg. Chem.*, 2017, **56**, 11230–11243; (b) N. Ghavale, S. T. Manjare, H. B. Singh and R. J. Butcher, *Dalton Trans.*, 2015, **44**, 11893–11900; (c) J. Jin, H. W. Shin, J. H. Park, J. H. Park, E. Kim, T. K. Ahn, D. H. Ryu and S. U. Son, *Organometallics*, 2013, **32**, 3954–3959; (d) E. Alvarado, A. C. Badaj, T. G. Larocque and G. G. Lavoie, *Chem.–Eur. J.*, 2012, **18**, 12112–12121; (e) K. Srinivas and G. Prabusankar, *Dalton Trans.*, 2017, **46**, 16615–16622; (f) H. R. Kim, I. G. Jung, K. Yoo, K. Jang, E. S. Lee, J. Yun and S. U. Son, *Chem. Commun.*, 2010, **46**, 758–760; (g) K. Srinivas, C. N. Babu and G. Prabusankar, *Dalton Trans.*, 2015, **44**, 15636–15644; (h) K. Srinivas and G. Prabusankar, *RSC Adv.*, 2018, **8**, 32269–32282.

2 (a) K. Srinivas, A. Sathyanarayana, C. N. Babu and G. Prabusankar, *Dalton Trans.*, 2016, **45**, 5196–5209; (b) H.-N. Zhang, W.-G. Jia, Q.-T. Xu and C.-C. Ji, *Inorg. Chim. Acta*, 2016, **450**, 315–320; (c) A. K. Sharma, H. Joshi, K. N. Sharma, P. L. Gupta and A. K. Singh, *Organometallics*, 2014, **33**, 3629–3639; (d) Y. B. Huang, W. G. Jia and G. X. Jin, *J. Organomet. Chem.*, 2009, **694**, 86–90; (e) G. Prabusankar, A. Mannem and N. Muthukumaran, *J.*

Organomet. Chem., 2019, **884**, 29–35; (*f*) A. K. Sharma, H. Joshi, R. Bhaskar and A. K. Singh, *Dalton Trans.*, 2017, **46**, 2228–2237.

3 G. K. Rao, A. Kumar, J. Ahmed and A. K. Singh, *Chem. Commun.*, 2010, **46**, 5954–5956.

4 D. J. Williams, K. M. White, D. VanDerveer and A. P. Wilkinson, *Inorg. Chem. Commun.*, 2002, **5**, 124–126.

5 J. Li, F. Jiang, B. Yang, X.-R. Song, Y. Liu, H.-H. Yang, D.-R. Cao, W.-R. Shi and G.-N. Chen, *Sci. Rep.*, 2013, **3**, 1998.

6 For the selected examples: (*a*) K. P. Bhabak and G. Mugesh, *Inorg. Chim. Acta*, 2010, **363**, 2812–2818; (*b*) K. P. Bhabak, K. Satheeshkumar, S. Jayavelu and G. Mugesh, *Org. Biomol. Chem.*, 2011, **9**, 7343–7350; (*c*) G. Roy, P. N. Jayaram and G. Mugesh, *Chem.–Asian J.*, 2013, **8**, 1910–1921.

7 J. H. Palmer and G. Parkin, *J. Am. Chem. Soc.*, 2015, **137**, 4503–4516.

8 M. Banerjee, R. Karri, K. S. Rawat, K. Muthuvel, B. Pathak and G. Roy, *Angew. Chem., Int. Ed.*, 2015, **54**, 9323–9327.

9 C. N. Babu, K. Srinivas and G. Prabusankar, *Dalton Trans.*, 2016, **45**, 6456–6465.

10 S. Yadav, S. T. Manjare, H. B. Singh and R. J. Butcher, *Dalton Trans.*, 2016, **45**, 12015–12027.

11 S. Yadav, H. B. Singh and R. J. Butcher, *Eur. J. Inorg. Chem.*, 2017, 2968–2979.

12 G. Raju, S. Vishwanath, A. Prasad, B. K. Patel and G. Prabusankar, *J. Mol. Struct.*, 2016, **1107**, 291–299.

13 A. Prasad, G. Raju, V. Sivalingam, A. Girdhar, M. Verma, A. Vats, V. Taneja, G. Prabusankar and B. K. Patel, *Sci. Rep.*, 2016, **6**, 39490.

14 K. Srinivas, P. Suresh, C. N. Babu, A. Sathyanarayana and G. Prabusankar, *RSC Adv.*, 2015, **5**, 15579–15590.

15 (*a*) S. Gondzik, S. Schulz, D. Bläser and C. Wölper, *Chem. Commun.*, 2014, **50**, 1189–1191; (*b*) P. Bora, B. Saikia and B. Sarma, *Cryst. Growth Des.*, 2018, **18**, 1448–1458.

16 A. Kellmann, *J. Phys. Chem.*, 1977, **81**, 1195–1198.

17 A. Elangovan, H. Chiu, S. Yang and T. Ho, *Org. Biomol. Chem.*, 2004, **2**, 3113–3118.

18 (*a*) A. Jegatha Christy and M. Umadevi, *Int. J. ChemTech Res.*, 2015, **8**, 383–390; (*b*) G. Prabusankar, N. Muthukumaran, M. Vaddamanu, G. Raju, M. Mannarsamy, K. Velappan, A. Sathyanarayana, Y. Masaya, S. Sugiyama, K. Hisano and O. Tsutsumi, *RSC Adv.*, 2019, **9**, 7543–7550.

19 A. Gafni and L. Brand, *Chem. Phys. Lett.*, 1978, **58**, 346–350.

20 (*a*) M. Goez, Cyclic and linear photoionizations of acridine derivatives and xanthone investigated by nanosecond laser flash photolysis, PhD thesis, Martin-Luther-University Halle-Wittenberg, 2005; (*b*) C. R. Ronda, Emission and excitation mechanisms of phosphors, in *Luminescence: From Theory to Applications*, ed. C. R. Ronda, Wiley-VCH Verlag GmbH & Co. KGaA, Weinheim, 2008, pp. 1–34.

21 J. Luo, Z. Xie, J. W. Y. Lam, L. Cheng, H. Chen, C. Qiu, H. S. Kwok, X. Zhan, Y. Liu, D. Zhu and B. Z. Tang, *Chem. Commun.*, 2001, 1740–1741.

22 J. Mei, N. L. Leung, R. T. Kwok, J. W. Y. Lam and B. Z. Tang, *Chem. Rev.*, 2015, **115**, 11718–11940.

23 S. Yamada, S. Yamaguchi and O. Tsutsumi, *J. Mater. Chem. C*, 2017, **5**, 7977–7984.

24 K. Fujisawa, S. Yamada, Y. Yanagi, Y. Yoshioka, A. Kiyohara and O. Tsutsumi, *Sci. Rep.*, 2015, **5**, 7934.

25 A. Sathyanarayana, N. Shin-ya, H. Kyohei, T. Osamu, S. Katam and G. Prabusankar, *Sci. China: Chem.*, 2018, **61**, 957–965.

26 R. Sakamoto, T. Iwashima, J. F. Kögel, S. Kusaka, M. Tsuchiya, Y. Kitagawa and H. Nishihara, *J. Am. Chem. Soc.*, 2016, **138**, 5666–5677.

27 J. Z. Zheng, J. W. Allen, D. E. Spence, W. E. Sleat and W. Sibbett, *Appl. Phys. Lett.*, 1993, **62**, 63–65.